



In situ XANES study of methanol decomposition and partial oxidation to syn-gas over supported Pt catalyst on SrTiO₃ nanocubes



Hui Wang^{a,c}, Junling Lu^b, Christopher L. Marshall^{a,*}, Jeffrey W. Elam^b, Jeffrey T. Miller^a, HongBo Liu^a, James A. Enterkin^d, Robert M. Kennedy^d, Peter C. Stair^e, Kenneth R. Poeppelmeier^e, Laurence D. Marks^f

^a Chemical Sciences and Engineering Division, Argonne, IL 60439, USA

^b Energy Systems Division, Argonne National Laboratory, Argonne, IL 60439, USA

^c Department of Chemical and Biological Engineering, University of Saskatchewan, Saskatoon, SK S7N 5A9, Canada

^d Graduate Student, Chemistry Department, Northwestern University, USA

^e Professor, Chemistry Department, Northwestern University, USA

^f Professor, Department of Material Sciences, Northwestern University, USA

ARTICLE INFO

Article history:

Received 11 November 2013

Received in revised form 31 January 2014

Accepted 10 February 2014

Available online 11 March 2014

Keywords:

Methanol

Decomposition

Partial oxidation

In situ XANES

SrTiO₃ nanocuboid

Platinum nanoparticle

ABSTRACT

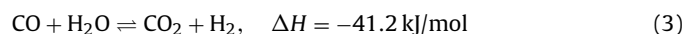
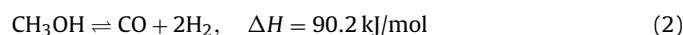
A catalyst of Pt nanoparticles was prepared by atomic layer deposition on SrTiO₃ nanocuboids and tested for methanol decomposition and partial oxidation. The catalyst had uniform nanoparticle size of 1.58 ± 0.37 nm and a Pt (1 1 1) surface. *In situ* X-ray absorption near-edge spectroscopy (XANES) measured in a temperature-programmed reduction showed that the Pt particles were easily reduced. However, the as-received catalyst, a reduced catalyst, and an oxidized catalyst all had catalytic activity, differing slightly in methanol conversion and product selectivity. *In situ* XANES also revealed that CO adsorbed on the Pt sites was the only observed surface species during both methanol decomposition and partial oxidation. It seemed that the breakage of CH and OH bonds overwhelmingly occurred once methanol was adsorbed, forming H₂ and adsorbed CO. The latter was then released from the catalyst surface or was oxidized to CO₂ when O₂ was present.

© 2014 Elsevier B.V. All rights reserved.

1. Introduction

The Institute of Atomic-Efficient Chemical Transformations (IACT) led by Argonne National Laboratory researchers focuses on key catalytic conversions that could improve the efficiency of producing fuels from biomass resources. Catalytic conversion of methanol (MeOH) into hydrogen or other value-added chemicals or energy forms plays an important role in biomass utilization because methanol can be produced from renewable sources such as lignocellulosic biomass and sugar, as well as from starch crops via biochemical or chemical processes [1].

Because of its high H-to-C ratio and absence of C–C bonds, methanol is an ideal onboard liquid hydrogen carrier for H₂ fuel cell vehicles. Hydrogen can be produced at relatively low temperatures by steam reforming and other reforming reactions:



Two major groups of catalysts, Cu-based alloys and Group VIII metals, have been used in investigations of steam reforming of methanol by Sá et al. [2]. Supported Cu catalysts must be reduced to form Cu metallic particles on the catalyst. Catalyst preparation must yield high values of Cu metal dispersion and surface area but small metallic particle size. Catalytic deactivation occurs mostly because of Cu oxidation and sintering, carbon formation, and/or formation of poisoning gases in the feed. Catalytic deactivation also results from CO formed during the reforming reactions. The reaction mechanism can involve one or two adsorbed molecules, depending on the support materials and preparation method. In the dual-molecule mechanism, two adsorbed methanol molecules form methyl formate. In the single-molecule mechanism, an adsorbed methanol forms formaldehyde on the catalyst surface. Either methyl formate or formaldehyde on the surface is hydrolyzed to form formic acid, and then the formic acid is decomposed to form hydrogen and CO₂. A reverse water-gas shift reaction is blamed for the formation of CO, which is harmful to the

* Corresponding author. Tel.: +1 630 252 4310; fax: +1 630 972 4408.

E-mail addresses: marshall@anl.gov, clmarshall@anl.gov (C.L. Marshall).

anodic catalyst in the low-temperature H₂ fuel cell. The Group VIII–X metal-based catalysts for the steam reforming of methanol are also reviewed in this paper, among which Pd supported on ZnO is the most commonly used [2]. Even for other supports, the addition of Zn greatly improves the catalytic selectivity and H₂ production rate. When used in steam reforming, the Pd metallic particles and PdZn alloy exhibit different reaction mechanisms. On the metallic Pd particles, the dehydrogenated formaldehyde is adsorbed on two sites with C and O atoms, and then is decomposed into CO and H₂. On the PdZn alloy particles, the dehydrogenated formaldehyde is adsorbed on one site with an O atom, followed by nucleophilic addition of water, formation of formic acid, and its decomposition. Compared with Cu-based catalysts, Pd–Zn catalysts are more stable due to their resistance to sintering and easy recovery from oxidation.

Because use of a direct methanol fuel cell for vehicle propulsion is simpler than converting methanol to hydrogen in a reformer and then hydrogen to electricity in a fuel cell [3], researchers have widely studied the decomposition of methanol on transition metal catalysts or supported transition metal catalysts, among which Pt is the most widely examined. Desai et al. used a periodic density functional theory (DFT) calculation to determine the methanol decomposition mechanism on the Pt (1 1 1) surface; in particular, they analyzed the interactions of the possible radicals such as molecular methanol, methoxide, hydroxymethyl, formaldehyde, formyl, CO, and H on an ideal and defect Pt (1 1 1) surface [4]. They concluded that methanol molecules are not activated by the ideal Pt (1 1 1) surface; while on the defect surface, an OH bond is likely to be broken to form methoxide, followed by its dehydrogenation via the formation of formaldehyde and formyl. After dehydrogenation, adsorbed CO and H are formed on the surface. The latter further desorbs to form H₂ but the former stays on the surface as a poisonous species. Niu et al. employed DFT with general gradient approximation to study the methanol decomposition mechanism on five surfaces: flat Pt (1 1 1), Pt defect, Pt step, Pt (1 1 0) (1 × 1), and Pt (1 1 0) (2 × 1) [5]. They observed that the decomposition of methanol on these surfaces begins with the activation and breakage of the OH bond, followed by the consecutive dehydrogenation of the methoxide, formaldehyde, and formyl on the Pt surfaces and ending with the formation of adsorbed CO and H. They also reported that the stereochemical configuration and bond length of the adsorbed species and the energy of the pathway change according to the different catalyst surface structures. Experimental studies do not always entirely agree with theoretical calculations, however. For example, using soft X-ray synchrotron photoelectron spectroscopy, Matolin et al. studied the methanol desorption on Pt particles supported on Ce (1 1 1)/Cu (1 1 1) and on an ion-eroded Pt (1 1 1) single crystal [6]. They found that the chemisorbed methoxy formed on both surfaces, which is consistent with the theoretical calculations. However, they also detected the partial C–O bond scission and the carbon formation. The same group extended their research to the Pt (1 1 0) (2 × 1) single crystal [7]. They observed CO adsorption as molecules form on the surface, but no trace of carbon on the crystal.

In Pt-based catalyst development for methanol decomposition to produce syn-gas, Brown and Gulari synthesized Pt/Al₂O₃ catalyst and a ceria-promoted Pt/Al₂O₃ catalyst using a single-step sol-gel method [8]. The optimum Pt and CeO₂ loading was found to be 9 and 10 wt %, respectively. The addition of ceria improved both methanol conversion and selectivity for H₂ and CO. The best catalyst completely avoided the methanation reaction. Although Brown and Gulari evaluated Pt/Al₂O₃ and Pt/CeO₂-Al₂O₃ catalysts of various compositions and compared their performance with commercial catalysts and other catalysts with other metals, they did not perform a mechanism study. Croy et al. investigated the pretreatment effect on methanol decomposition and oxidation over a catalyst of Pt nanoparticles supported on ZrO₂, which was synthesized using

a so-called “micelle method,” where the Pt precursor was first dissolved in self-prepared nano-cages of a polymer solution and then loaded onto ZrO₂ nanoparticles (NPs) [9]. The size of the Pt NPs was controlled by the size of the cages, and the latter was controlled by the functional groups of the polymer. It was interesting to observe that the catalyst pretreated in O₂/H₂ mixture resulted in the best activity for methanol decomposition, followed by the catalyst pretreated in O₂ and He. The catalyst pretreated in H₂ did not show good activity. The pretreatment did not affect the activity of the oxidation reaction. Croy et al. believe that the Pt oxide is of help in the maintenance of clean, stable, and active Pt NPs [9]. But the oxide is easily reduced with the formed H₂ and facilitates the decomposition reaction. The same group extended the studies to include the decomposition of other alcohols [10]. Ubago-Perez et al. prepared a Pt catalyst supported by activated carbon by adsorbing Pt precursor solutions onto self-made activated carbon particles followed by solvent removal and drying [11]. A linear relationship was found between the turn-over frequency of methanol decomposition and the Pt NP size, which can be controlled by the pretreatment gases used. Helium-treated catalyst had NPs with narrower particle size distribution and smaller average size and higher surface Pt dispersion, which led to lower decomposition activity. Hydrogen-treated catalyst, however, had NPs with broader particle size distribution and greater average size and lower surface Pt dispersion, which led to higher activity. Ubago-Perez et al. concluded that larger particles facilitated higher activity to methanol decomposition and that the formed CO suppressed the smaller Pt particles.

The IACT researchers earlier developed a Pt/SrTiO₃-nanocuboid catalyst. The catalyst support consists of single-crystal nanocubes of SrTiO₃ with an edge length of 60–120 nm. It was synthesized using sol-precipitation coupled with a hydrothermal procedure or a molten salt procedure [12]. The platinum was introduced onto the support by atomic layer deposition (ALD), such that the Pt particles are evenly distributed and their size is controlled by the number of ALD cycles [13]. Because of the unique properties of the catalyst, *i.e.*, nonporous single-crystal support and evenly dispersed Pt nanoparticles with known surface structure, we use it as a model for the study of methanol decomposition and partial oxidation. By combining catalytic performance tests and the results of *in situ* X-ray absorption near-edge spectroscopy (XANES), we hope to deepen the understanding of the mechanism of methanol decomposition and partial oxidation over the Pt/SrTiO₃-nanocuboid catalyst made by ALD. This paper reports the result of this study.

2. Experimental

2.1. Catalyst preparation

SrTiO₃ nanocuboids were synthesized by using sol-precipitation combined with hydrothermal treatment [12]. About 80 mL of an aqueous solution containing stoichiometric amounts of Sr and Ti was prepared from Sr(OH)₂·8H₂O and TiCl₄ as metallic precursors. Co-precipitation of SrTiO₃ was induced by adding about 5 g of NaOH pellets to the above bimetallic precursor solution. Dissolution of the NaOH pellets produced a highly viscous suspension, which was subsequently transferred to a 125 mL Teflon-lined autoclave and heated at 240 °C for 36 h. The solution was filtered, and the product washed thoroughly with double-deionized water and dried at 80 °C for 24 h, yielding SrTiO₃ nanocuboids.

The Pt atoms were deposited onto the SrTiO₃ nanocuboids using ALD [13–15]. About 0.25 g of the SrTiO₃ nanocuboids powder was spread in a stainless steel tray. The powder was covered by a stainless steel mesh that allowed easy access by the ALD precursors and contained the powder while being cleaned *in situ* with a 400 mL/min flow of an ozone-oxygen (10% ozone) mixture

at 300 °C. The Pt ALD was conducted using alternating 200-s exposures to 0.05 torr methylcyclopentadienyl trimethylplatinum (MeCpPtMe₃) and 0.20 torr oxygen at 300 °C. The viscous-flow ALD reactor was operated with a constant 90 mL/min flow of ultrahigh purity nitrogen (99.995%) carrier gas at a pressure of 0.90 torr. Nitrogen purge periods of 50 s were used between reactant exposures.

The platinum catalyst samples were prepared using one Pt ALD cycle over SrTiO₃. The catalyst is denoted as 1cPt/SrTiO₃, where 1c represents 1 ALD cycle. The sample mass was measured with an analytical balance before and after the Pt ALD to determine the Pt loading.

2.2. Catalyst characterization

Transmission electron microscopy (TEM) and high-resolution electron microscopy (HREM) of the 1cPt/SrTiO₃ nanocuboids were performed with a JEOL JEM-2100F electron microscope operated at 200 kV, as described by Enterkin et al. [14]. We did not conduct other characterization. However, the analysis results by others of the same catalysts, sometimes with various ALD cycles, can be found in previous papers. The methods are briefly described here.

The specific surface areas were measured at –196 °C using a Micromeritics ASAP 2010 analyzer. Samples were degassed overnight at 200 °C under vacuum prior to the measurement. X-ray diffraction patterns were collected using a Rigaku DMAX diffractometer in the Bragg–Brentano configuration operated at 20 mA and 40 kV. For that analysis, CuK α radiation ($\lambda = 1.5418 \text{ \AA}$) filtered with Ni was employed. The step size and collection time were 0.025° and 1 s per step, respectively. Platinum dispersion (the percentage of platinum atoms at the surface) was calculated from CO chemisorption data. *In situ* reduction of the sample was performed in a Zeton Altamira AMI-100 by heating to 300 °C with 3% H₂ in argon, cooling to –50 °C in argon, and pulsing with CO gas. After each CO pulse in the gas, output was measured by a Dycor Dymaxion quadrupole mass spectrometer. The CO adsorption on SrTiO₃ nanocuboids was measured to be 2.18 CO molecules adsorbed per nm² of SrTiO₃ surface. This factor was used to correct the Pt dispersion for the

Pt/SrTiO₃ nanocuboid catalysts. With a hemispherical model for the platinum particles (which is not the true particle morphology, but close enough for particle size estimation), the average Pt particle radius was calculated. The resulting particle would expose the proper amounts of platinum and cover the correct amount of support surface to account for the observed CO adsorption.

2.3. Catalytic performance tests for methanol decomposition and partial oxidation

The catalytic performance was tested with methanol decomposition and partial oxidation reactions using a quartz tubular reactor (c.a. 1.27 mm i.d.). About 0.010 g of the catalyst diluted with about 0.090 g of silicon carbide was loaded. Three catalysts were used in the test: the as-received catalyst, *i.e.*, the catalyst made from ALD without any treatment before the test; the reduced catalyst, *i.e.*, the as-received catalyst that had been reduced in H₂/Ar (3.5% H₂, 206 mL/min) at 400 °C for 2 h before the test; and the oxidized catalyst, *i.e.*, the as-received catalyst that had been oxidized in O₂/Ar (19.0% O₂, 20 mL/min) at 500 °C for 2 h before the test. The reduction or oxidation was conducted in the same reactor before methanol decomposition or partial oxidation reaction. The reduction temperature, 400 °C, and the oxidation temperature, 500 °C, were chosen based on a paper by Huizinga et al. [16], who indicated that their Pt/TiO₂ catalyst was fully reduced by 400 °C and completely oxidized up to 500 °C. For the decomposition reaction, liquid methanol was injected by a syringe pump (Issco Model 100 DM) into the argon gas stream to form a gas mixture that contained 4.4% (v/v) methanol. For the partial oxidation (or oxy-reforming) reaction, the balance gas was an oxygen-argon (0.976% O₂) mixture. The flow rate of the gases was controlled by mass flow controllers (calibrated to mL/min at standard temperature and pressure), and the gas hourly space velocity (GHSV) was 1250–1300 L/g_{cat}/h. The reaction temperature was controlled by an Omega Model CN375 temperature control unit. The composition of the effluent gas from the reactor was determined on an Agilent model 5890 gas chromatograph (GC) equipped with a thermal conductivity detector and 10-port valve that acted both as the sampling device and the column

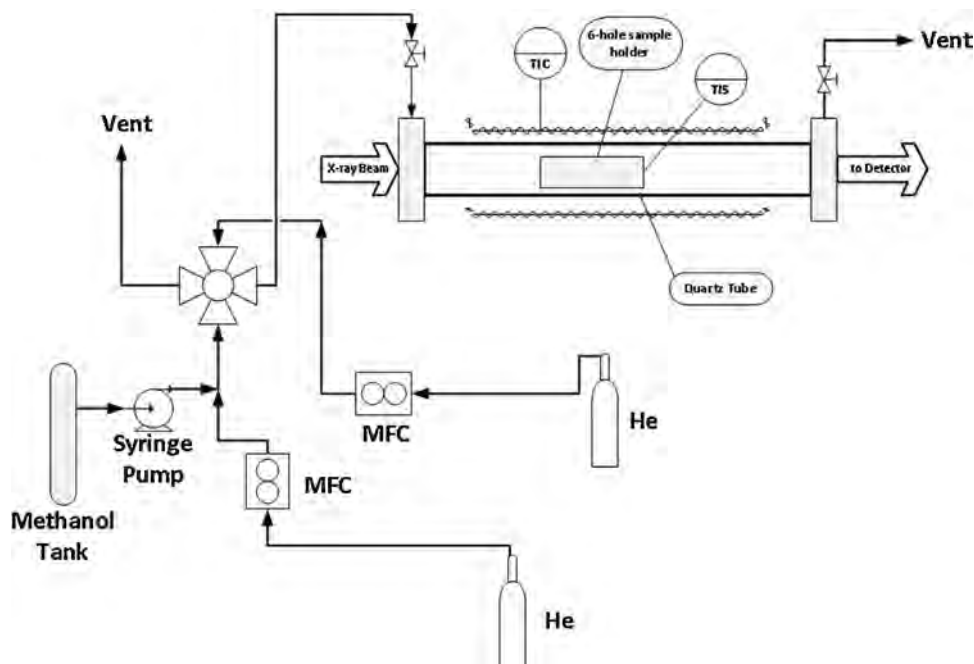


Fig. 1. Schematic of a catalytic reactor that can be incorporated with *in situ* X-ray absorption spectroscopy (XAS) measurement in a synchrotron beamline. MFC: mass flow controller; TIC: temperature controller; TIS: temperature sensor.

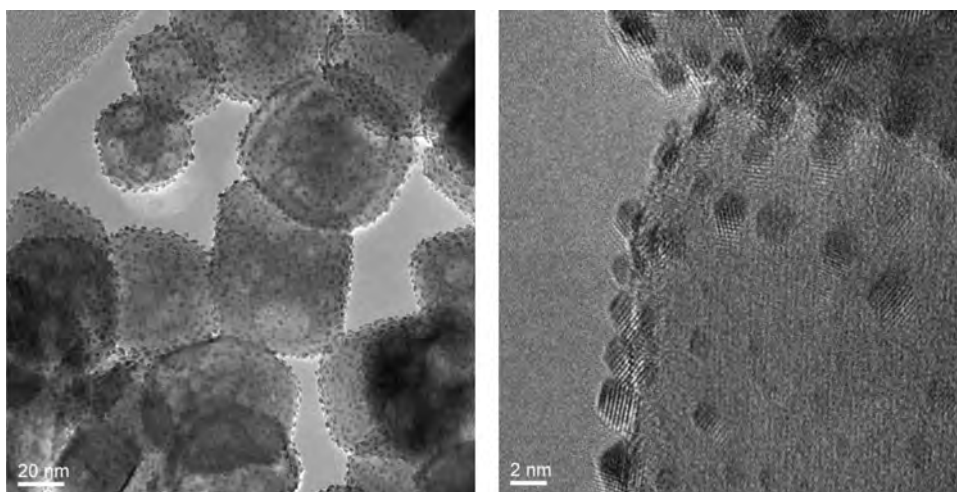


Fig. 2. TEM images of 1cPt/SrTiO₃ catalyst as received: (a) low perspective and (b) high perspective.

switching valve. The column set consisted of a molecular sieve and a porous polymer PLOT column. Argon was used as carrier gas.

Each test lasted 80–90 min, during which five GC analyses were performed. The results from the last four analyses were averaged and used in the conversion and selectivity calculation. Because the reaction component was no more than 5% (v/v), the molar flow rate, F , of every component was simply calculated by multiplying the total gas flow rate by its mole fraction. The conversion of methanol and O₂ was calculated by

$$X = \frac{F_{\text{in}} - F_{\text{out}}}{F_{\text{in}}} \quad (4)$$

The selectivity of the product components (H₂, CO, CO₂, and CH₄) based on methanol was calculated by

$$S = \frac{F_{i,\text{out}}}{n(F_{\text{MeOH},\text{in}} - F_{\text{MeOH},\text{out}})} \quad (5)$$

where $n = 2$ for H₂ and $n = 1$ for other components.

2.4. *In situ* XANES measurements for temperature-programmed reduction and methanol decomposition and partial oxidation

Although a quartz tube reactor with 6-hole shooter has been commonly used at the Advanced Photon Source (APS) in Argonne National Laboratory for catalysis research, the *in situ* system must be implemented such that the switch of reactants can be conducted automatically, and the catalyst treatment or the catalytic reaction can be performed while an X-ray absorption spectroscopy (XAS) measurement is conducted. A schematic of the *in situ* reactor incorporated with an APS beamline is shown in Fig. 1. The XAS for the Pt L₃-edge during the temperature-programmed reduction (TPR) of the 1cPt/SrTiO₃ catalyst was conducted at the MRCAT 10 ID (insertion device) beamline at APS. The catalyst samples (6–9 mg) were diluted with 15–25 mg silica gel, packed in a 6-hole shooter, pre-treated in an O₂/He (5% O₂) mixture at 500 °C for 1 h, and cooled to room temperature. Then, the tube reactor was moved into a hutch aligned with the beamline. The temperature was programmed to start at room temperature and increased at a rate of 3 °C/min while a 3.5% H₂/He gas flowed through the reactor. A XANES spectrum was obtained about every 4.6 min until the temperature reached 250 °C or no more change was found between the next two spectra. *In situ* Pt L₃-edge XANES of the catalyst during methanol decomposition and partial oxidation was conducted at the MACAT 10 BM (bending magnet) beamline of APS. In order to mimic the catalyst evaluation experiments at the beamline, we followed the same

procedure used in the catalyst evaluation, though some steps were modified to adapt to the XAS measurements. For example, the space velocity could not be the same as used in the catalyst evaluation due to a different reactor size. In addition, when the temperature and/or gas composition were changed, the system was maintained for 1 h under the new condition, allowing steady state to be reached before the XANES scan was performed. Thus, we believe the surface species would not change due to the modification because they are determined by the reaction temperature and the reactant compositions at steady state. For the *in situ* XAS measurement, ionization chambers were used to measure the transmittance of the photons. They were optimized for the maximum current with linear response (ca. 10¹⁰ photons detected/s) using a mixture of N₂ and He in the incident X-ray detector and a mixture of ca. 20% Ar in N₂ in the transmission X-ray detector. A third detector in the series collected a reference spectrum (Pt foil) simultaneously with each measurement for energy calibration.

2.5. XAS data analysis

WINXAS 3.2 standard procedures were used to analyze the XAS data. Normalized, energy-calibrated Pt L₃ edge XANES spectra were obtained. For the TPR data, the XANES spectra were fit with to a linear combination of Pt metal foil (Pt⁰), Na₂Pt(OH)₆ (Pt⁴⁺), and 1 nm Pt/silica catalyst which had been oxidized at room temperature (Pt²⁺). For the data obtained during reaction, reference XANES spectra for CO adsorption corresponding to the coverage at room temperature and the reaction temperature were measured. The Δ XANES spectra were obtained by subtracting the XANES spectrum of the reduced 1cPt/SrTiO₃ catalyst in H₂ from that with different reaction gases at the reaction temperature. To determine the coverage of CO, the XANES of the CO adsorption on the reduced catalyst at room temperature was used as the reference for 100% CO coverage.

3. Results and discussion

3.1. Catalyst characterization

The characterization results of the physical and morphological properties of the SrTiO₃ nanocuboids and the Pt/SrTiO₃ catalyst were discussed earlier [12–15]. In summary, the SrTiO₃ nanocuboids made by the sol-precipitation/hydrothermal treatment method are nonporous, single-crystal, cubic-shaped particles of an average edge length of 60 nm and BET surface area of 20 m²/g. The formation of Pt particles on the nanocuboids increases the

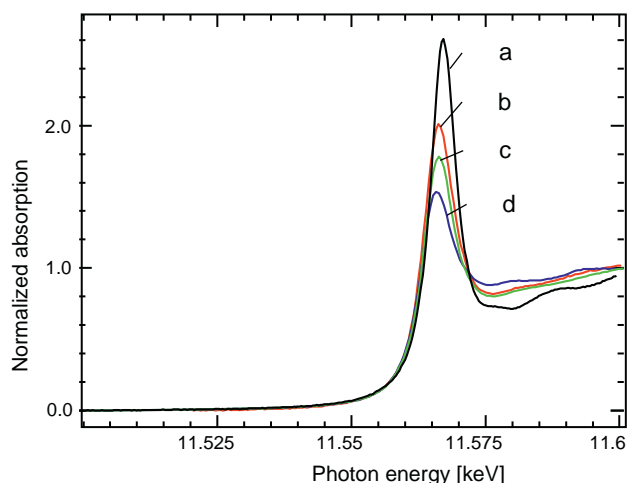


Fig. 3. Pt L3 XANES spectra of Pt⁴⁺ (Na₂Pt(OH)₆) standard (a), as-received catalyst (c), catalyst oxidized at 500 °C and then cooled to room temperature (b), and catalyst oxidized at 500 °C and then cooled to 250 °C (d).

specific surface area – after 5 cycles of Pt ALD, the specific area becomes 31 m²/g. The specific area of 1cPt/SrTiO₃ was not measured in this study. The X-ray diffraction pattern shows broadening of the (1 1 1) reflection of the perovskite phase with the overlap of the Pt⁰ (1 1 1) reflection. The metal dispersion measured by CO chemisorption is 75%. A TEM image of 1cPt/SrTiO₃ that we scanned in this study is given in Fig. 2. With one cycle of Pt ALD 4.7 wt% Pt was loaded onto the cuboids particles [14]. The histogram of Fig. 2(a), given in support documents, shows an average Pt nanoparticle size of 1.58 ± 0.37 nm. The particles are well dispersed, and the size distribution is very narrow. The lattice spacing between neighboring fringes in the Pt particle areas in Fig. 2(b) is about 0.250 nm, which is close to the distance between the two adjacent (1 1 1) planes of face-centered cubic (fcc) Pt (0.237 nm) [17].

3.2. Ex situ XANES analysis of 1cPt/SrTiO₃ catalyst

Fig. 3 shows the XANES spectra of the 1cPt/SrTiO₃ catalyst as-received (spectrum c), and oxidized in O₂/He mixture (b and d), along with a spectrum of a standard Na₂Pt(OH)₆ for Pt⁴⁺ (a). The difference between spectra b and d is that the scanning of the former took place at room temperature and that of the latter at 250 °C, the reaction temperature. Linear XANES fitting with another standard spectrum for Pt²⁺ (not shown) was used to estimate the Pt⁴⁺ and Pt²⁺ contents in the catalyst after various pretreatments, which are as-received (15% Pt⁴⁺, 85% Pt²⁺), oxidized but scanned at room temperature (42% Pt⁴⁺, 58% Pt²⁺), and oxidized but scanned at 250 °C (1% Pt⁴⁺, 99% Pt²⁺). We wondered whether the temperature at which the XAS was conducted for the oxidized catalyst had an effect on the content of the Pt species, and whether cooling the oxidized catalyst from 500 °C to the reaction temperature of 250 °C resulted in less Pt⁴⁺ content. Rossin studied the Pt/γ-Al₂O₃ catalyst reduction and oxidation using X-ray photoelectron spectroscopy and found that the oxidation above 410 °C resulted in Pt reduction [18]. Huizinga et al. explained this phenomenon as due to the decomposition of PtO₂ into Pt and O₂ and found that a TiO₂ support lowered the decomposition temperature [19]. We did not see, however, the Pt formation during 1cPt/SrTiO₃ oxidation. Cooling the oxidized catalyst to 250 °C made nearly all Pt present as Pt²⁺.

3.3. In situ XANES of TPR

Fig. 4 shows the changes in the temperature and the oxidation states of Pt vs. time during the TPR experiment with 1cPt/SrTiO₃

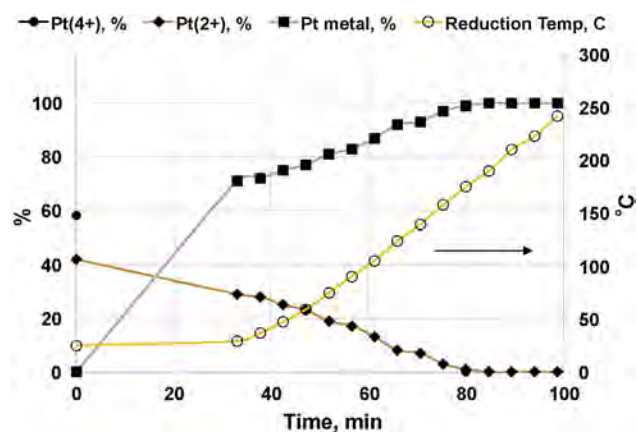


Fig. 4. Pt oxidation state change against reduction temperature from XANES measured during *in situ* TPR.

catalyst. The Pt L3 XANES spectra obtained during TPR were fitted with the spectra of the standard Pt⁴⁺, Pt²⁺, and Pt metal foil (Pt⁰) using the software WinXas 3.2. After 1 h pretreatment at 500 °C in the 5% O₂/He flow followed by cooling to room temperature, the 1cPt/SrTiO₃ contained 58% Pt⁴⁺ and 42% Pt²⁺. Once the sample had been contacted with hydrogen even at room temperature, all the Pt⁴⁺ was reduced, along with reduction of some Pt²⁺, resulting in Pt²⁺ and Pt metal in the catalyst. Before the temperature increase, the catalyst contained 30% Pt²⁺ and 70% Pt⁰. Then, the Pt⁰ content increased and the Pt²⁺ content decreased as the reduction temperature ramped up. At 180 °C, Pt was fully reduced into Pt⁰. Later, in the *in situ* XANES study of the reaction, the comparison between the spectra of the catalyst reduced in the H₂/He mixture at 250 °C for 1 h and the Pt foil confirmed this observation. The easy change from Pt⁴⁺ into Pt²⁺ during reduction might imply an easy opposite process in oxidation. This finding may be used to explain the remaining question: why cooling the oxidized 1cPt/SrTiO₃ to room temperature leads to more Pt⁴⁺ but cooling to 250 °C leads to nearly all Pt²⁺.

3.4. Catalytic performance during methanol decomposition and partial oxidation

To begin, the SrTiO₃ nanocuboid substrate was tested with methanol decomposition and partial oxidation at 250 °C. The methanol conversion was 0.5% for the decomposition reaction, but no H₂ or CO was detected by the GC. However, for partial oxidation where 0.976% O₂ was present in the feed gas, nearly 1% methanol conversion and a trace amount of H₂ and CO₂ were observed. The substrate is practically inactive to both reactions. Fig. 5 shows the methanol conversion and selectivity for hydrogen, CO, and methane in methanol decomposition over the 1cPt/SrTiO₃ catalyst in three forms: as-received, reduced, and oxidized. The catalytic methanol conversion of the three forms decreases in the order as-received (25%), reduced (19%), and oxidized (15%). The H₂ selectivity and CO selectivity over the reduced and oxidized catalysts are also lower compared with those of the as-received catalyst. However, the selectivity for H₂ and CO over the reduced and oxidized catalysts only differs slightly. A trace amount of methane was detected for the as-received and reduced catalysts. It is worth noting that methane was not detected in the reaction supported by the oxidized catalyst.

Fig. 6 shows the performances of the three 1cPt/SrTiO₃ forms in the partial oxidation reaction, *i.e.*, oxy-reforming with a small amount of O₂ in the Ar feed gas. The as-received and reduced catalysts maintained similar methanol conversion, but the oxidized one led to lower conversion. The order of H₂ selectivity of the three

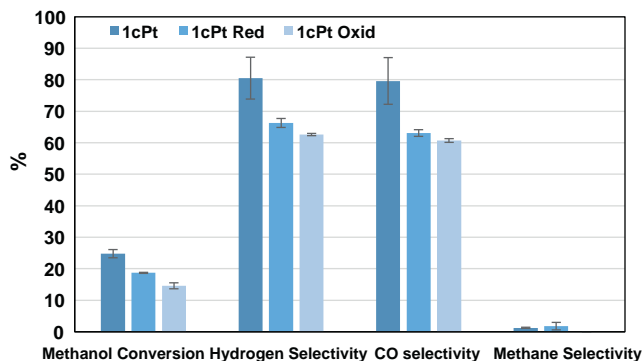


Fig. 5. Methanol conversion and product selectivity of methanol decomposition on 1cPt/SrTiO₃. Reaction condition: 250 °C, 0.010 g catalyst, 1300 L/g/h GHSV.

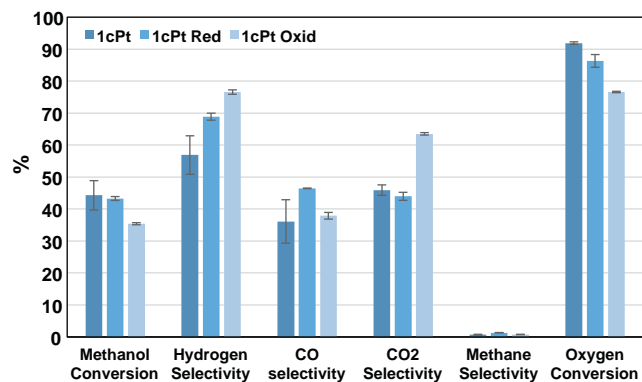


Fig. 6. Methanol conversion and product selectivity of methanol oxy-reforming on 1cPt/SrTiO₃. Reaction condition: 250 °C, 0.010 g catalyst, 1300 L/g/h GHSV.

catalyst forms was as-received < reduced < oxidized. The reduced catalyst resulted in greater CO selectivity (by 8–10 percentage points), whereas the oxidized catalyst favored more CO₂ selectivity (by 15–20 percentage points). The order of O₂ conversion of the three catalyst forms was as-received > reduced > oxidized. A trace amount of CH₄ was formed by all three types of the catalyst, indicating that partial oxidation is different from the decomposition reaction where the oxidized catalyst did not facilitate CH₄ formation.

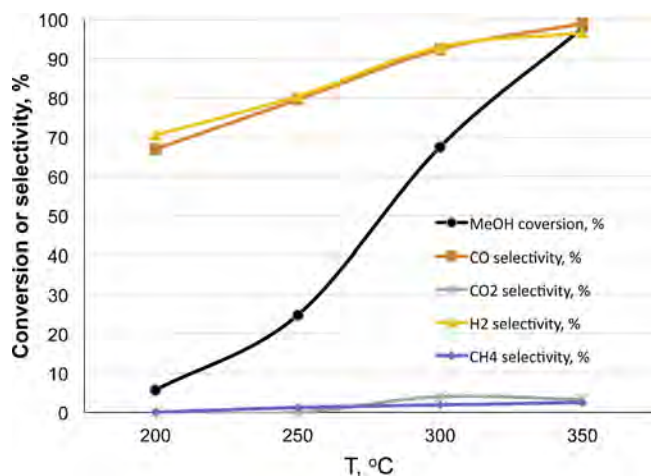


Fig. 7. Reaction temperature effect on methanol conversion and production selectivity for methanol decomposition on 1cPt/SrTiO₃. Reaction condition: 0.010 g catalyst, 1300 L/g/h GHSV.

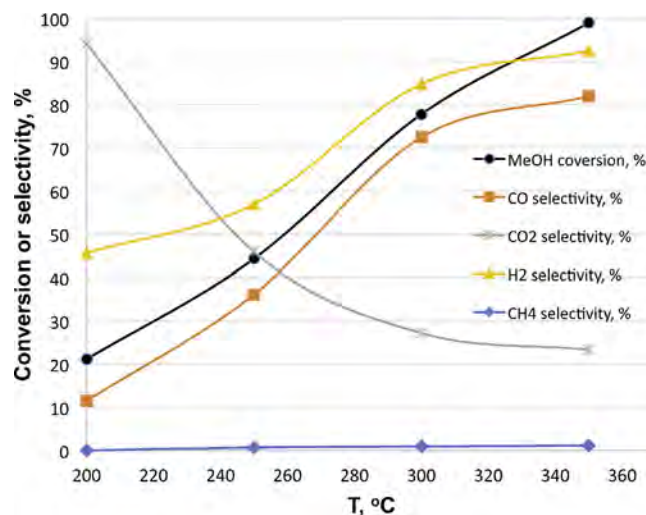


Fig. 8. Reaction temperature effect on methanol conversion and production selectivity for methanol oxy-reforming on 1cPt/SrTiO₃. Reaction condition: 0.010 g catalyst, 1300 L/g/h GHSV.

Fig. 7 shows the methanol conversion and selectivity for CO, CO₂, H₂, and CH₄ in methanol decomposition over the as-received 1cPt/SrTiO₃ catalyst at different temperatures. The methanol conversion increased rapidly from about 6% at 200 °C (473 K) to nearly 98% at 350 °C (623 K). Over the entire temperature range of the experiment, the selectivity for H₂ and that for CO were maintained at equal levels, which improved from 70% at 200 °C to nearly 100% at 350 °C. At lower H₂ and CO selectivity, however, no other products were found, except for a very small amount of methane and CO₂ at high temperatures (1–2.5% methane at 300 and 350 °C and 3–4% CO₂ at 250, 300, and 350 °C). In other words, the masses cannot be well balanced at low temperature.

Fig. 8 shows the results of methanol conversion and selectivity for CO, CO₂, H₂, and CH₄ over the as-received 1cPt/SrTiO₃ catalyst during methanol partial oxidation in the presence of O₂ at different temperatures. At 200–300 °C, the methanol conversion in the presence of O₂ was higher than that of the decomposition (Fig. 7). At 350 °C, both methanol and oxygen conversions reached nearly 100%. The selectivity for H₂ and CO both increased with temperature. However, unlike the decomposition reaction, the selectivity for H₂ was greater than that for CO, the difference being the greatest (factor of two) at 200 °C. This difference suggests that part of the CO produced is oxidized to CO₂ after the H atoms are extracted from the methanol molecules. The CO₂ selectivity dropped from 94% at 200 °C to 23% at 350 °C. The conversion of the O₂ from the feed was nearly 100%, and the CO₂ selectivity based on O₂ was 100% as well. This result indicates that the drop in CO₂ selectivity was due to the greater percentage of converted methanol at higher temperatures and not enough O₂ for further oxidation. This observation also supports the hypothesized two-step CO₂ formation. Production of CH₄ in a small amount was also observed at 250 °C and above. The amount was less than that produced in the decomposition reaction at corresponding temperatures.

3.5. In situ XANES of methanol decomposition and partial oxidation over 1cPt/SrTiO₃

Fig. 9 compares the XANES spectra obtained after the 1-h methanol decomposition over as-received, reduced, and oxidized 1cPt/SrTiO₃ catalysts at 250 °C. Also given is the XANES spectrum after 1-h CO adsorption on the as-received catalyst at the same temperature. The Pt L₃ XANES for as-received 1cPt/SrTiO₃ catalyst (red curve) during methanol decomposition had a stronger,

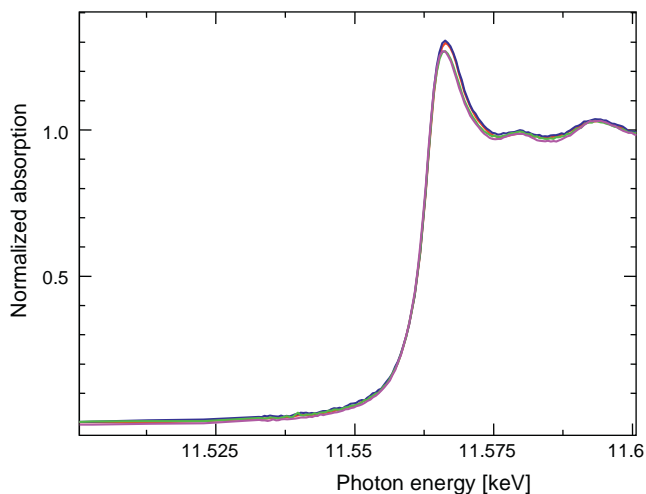


Fig. 9. Pt L3 XANES spectra of *in situ* methanol decomposition over as-received (red), reduced (green), and oxidized (blue) 1cPt/SrTiO₃ catalyst compared with that of CO adsorption on the as-received catalyst. (For interpretation of the references to color in this figure legend, the reader is referred to the web version of the article.)

higher-energy white line compared with spectra for the reduced and oxidized catalysts in reaction, which are the same (green and blue). Fig. 10 also shows that for the as-received catalyst, the XANES obtained during partial oxidation exactly overlapped with that obtained during CO adsorption (red and blue). In effect, regardless of the pretreatment, the XANES of the catalysts during the reaction was simply the same with the spectra when they adsorbed CO (spectra not given), indicating that adsorbed CO is the dominant surface species during methanol decomposition over the 1cPt/SrTiO₃ catalyst. This phenomenon was repeated in partial oxidation reactions. However, unlike the obvious difference of the XANES spectra for methanol decomposition between the as-received catalyst on the one hand and the reduced and oxidized catalyst on the other (Fig. 9), the partial oxidation of methanol over the three forms of the catalyst resulted in very similar XANES (Fig. 10).

The Δ XANES spectra (scanned at 250 °C) of the CO adsorption over the as-received, reduced, and oxidized catalyst are shown in Fig. 11. According to Wu et al., the intensity decrease below

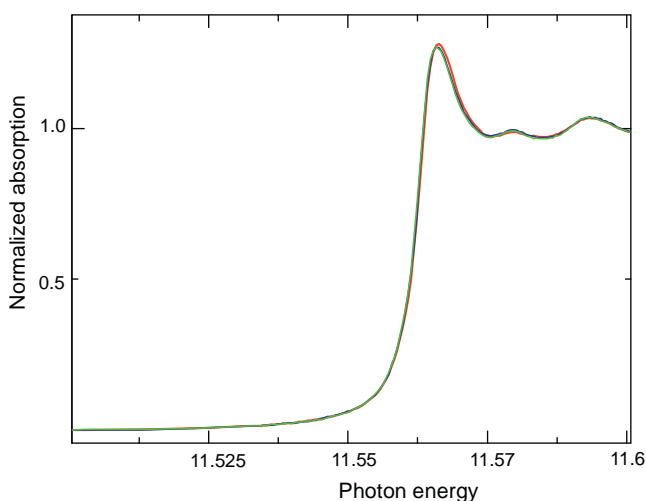


Fig. 10. Pt L3 XANES spectra of *in situ* methanol partial oxidation over as-received (red), reduced (blue), and oxidized (green) 1cPt/SrTiO₃ catalyst. (For interpretation of the references to color in this figure legend, the reader is referred to the web version of the article.)

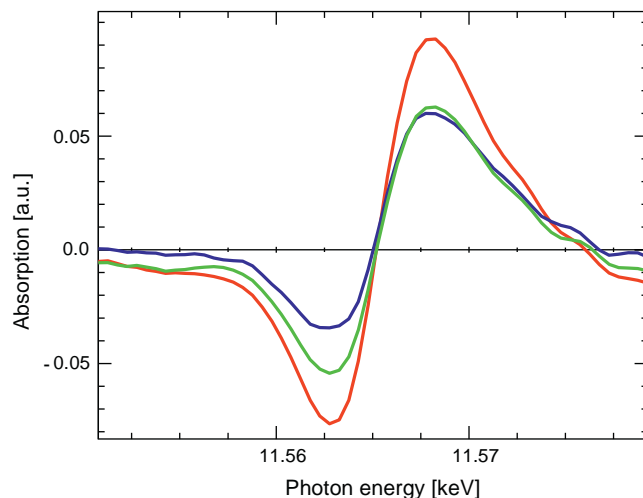


Fig. 11. Δ XANES spectra of Pt L3 after CO adsorption at 250 °C over as-received (red), reduced (blue), and oxidized catalyst (green). (For interpretation of the references to color in this figure legend, the reader is referred to the web version of the article.)

the inflection point represents the higher edge energy (or higher oxidation states), and the intensity increase after the inflection point is proportional to the increased spectrum intensity beyond the edge [19]. The intensity decrease order of the catalyst is as-received > oxidized > reduced. Linear fitting of XANES with CO adsorption on the reduced catalyst at room temperature, representing 100% CO coverage, gives the relative CO coverage at 250 °C, one of the reaction temperatures. The results are given in Table 1. The CO coverage on the reduced and oxidized catalyst is about the same (50%), and that of the as-received catalyst is about 1.5 times greater. The catalyst before any pretreatment, either reduction or oxidation, has more surface Pt. Fig. 12 (a and b) shows the Δ XANES spectra (scanned at 250 °C) of the methanol decomposition and partial oxidation over the catalysts with respect to the XANES spectrum of the reduced catalyst, respectively. It is interesting that the oxidized catalyst showed the least intensity before the inflection point. It seemed that this catalyst had been more reduced than the others during the reactions. In the decomposition reaction, the as-received and the reduced catalysts appeared to have the same intensity before the inflection point. But in partial oxidation, the order of the reduced Pt content appeared to be: oxidized > reduced > as-received catalyst. The CO coverage during the methanol reactions is also given in Table 1. The reduced and oxidized catalysts facilitate the same coverage; the as-received catalyst has about 1.5 times more CO coverage. For each catalyst, the CO coverage during the methanol reactions is comparable to that in CO adsorption.

4. Discussion

Comparing with some recently reported results obtained with supported Pt catalyst, Table 2 shows that the SrTiO₃ cuboid-supported Pt catalyst has very high reaction activity to methanol decomposition and partial oxidation. For example, Brown et al.

Table 1
CO coverage during CO adsorption, methanol decomposition, and methanol partial oxidation calculated from XANES fitting.

	As-received	Reduced	Oxidized
CO adsorption	0.73	0.48	0.52
MeOH decomposition	0.72	0.45	0.46
MeOH oxy-reforming	0.60	0.42	0.43

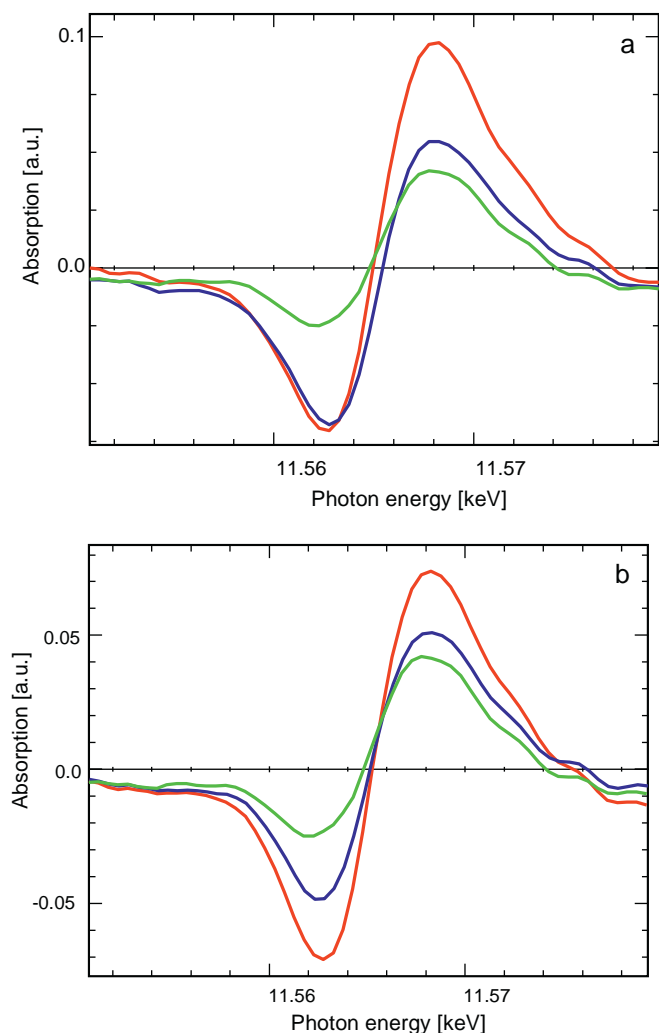


Fig. 12. Δ XANES spectra of Pt L3 after methanol decomposition (a) and partial oxidation (b) at 250 °C over as-received (red), reduced (blue), and oxidized catalyst (green). (For interpretation of the references to color in this figure legend, the reader is referred to the web version of the article.)

studied ceria-promoted Pt/Al₂O₃ catalyst for methanol decomposition [8]. They reported that the methanol conversion rates at 200, 250, and 300 °C are 18.8, 52.5, and 56.9 $\mu\text{mol/g/s}$, respectively. Mostafa et al. reported a ZrO₂-supported Pt catalyst for low carbon alcohol decomposition [10]. Reading from Fig. 6 in their article, we determined the methanol decomposition rates at 200, 250, and 300 °C to be 0.2, 2.9, and 5.9 $\mu\text{mol/g/s}$, respectively. Ubago-Perez et al. developed an activated-carbon-supported Pt catalyst that achieved a methanol decomposition rate of 3.39 $\mu\text{mol/g/s}$ at 200 °C [11]. The corresponding activity values (Table 2) for the

Table 2
Reaction activity ($\mu\text{mol/g cat/s}$) of methanol decomposition on various catalysts.

Catalyst	This study Pt/SrTiO ₃ -cuboids 4.7 wt%	Brown et al. [8] Pt/CeO ₂ -Al ₂ O ₃ 5 wt%	Mostafa et al. [10] Pt/ZrO ₂ 2 wt%	Ubago-Perez et al. [11] Pt(A)/carbon 2 wt%
GHSV	1300 L/g/h	126 L/g/h	30 L/g/h	18 L/g/h
200 °C	40.0	18.8	0.2	3.39 ^a
250 °C	175	52.5	2.9	
300 °C	477	56.9	5.9	
350 °C	691			

^a According to Fig. 6 in this article, the conversion of 2% Pt(A)/carbon catalyst is about 40%, which is translated to this activity. However, in the text, it says that about 45% methanol conversion was reached with the Pt(A)/carbon catalyst pretreated under H₂ flow at a reaction temperature of 200 °C.

as-received catalyst in our study are much higher: 40.0, 175, and 477 $\mu\text{mol/g/s}$ at 200, 250, and 300 °C. The major products from the decomposition reaction over 1cPt/SrTiO₃ are H₂ and CO in the ratio of 2:1, which was also observed by other researchers [9–11]. A trace amount of CO₂ is produced at high temperature (300 and 350 °C). We also observed the formation of methane (CH₄) in trace amount. By comparison, Ubago-Perez et al. did not detect any other products than CO and H₂ [11]. Brown et al. reported the formation of CH₄ at 360 °C and higher and attributed it to methanation [8]. Mostafa et al. showed a trace amount of CO₂ formation [10]. The high Pt metal dispersion (75%) achieved by ALD may be the major contribution to the high conversion rate of our catalyst in methanol decomposition because CO coverage during the reaction (Table 1) has a similar trend to the methanol conversion (Fig. 5) This observation is different from that of Ubago-Perez et al., who treated their Pt/carbon catalyst in He and H₂ to get high and low metal dispersion catalysts, respectively. They found that the low Pt dispersion catalyst led to high conversion [11]. Ubago-Perez et al. later also studied the partial oxidation of methanol [20]. The reported reaction rate at 200 °C was 5.09 $\mu\text{mol/g/s}$. Although this reaction rate is much lower than ours for partial oxidation, Ubago-Perez et al. observed the same trend of conversion and product selectivity with temperature as shown in our Fig. 8. Note that they used a similar O₂/CH₃OH ratio (0.2) to the one we used.

Table 3 shows the methanol conversion rate and the production rate of H₂, CO, and CO₂ as a function of temperature. The production of CO competes with that of CO₂ at 200 and 250 °C, but not all O₂ was used. It can be seen that the provision of O₂ constrains the formation of CO₂ at higher temperatures. All of the CO would have turned into CO₂ if sufficient O₂ had been present. Relative to the other catalysts, the as-received 1cPt/SrTiO₃ exhibits better performance in terms of methanol conversion and H₂ and CO selectivity in both methanol decomposition and partial oxidation.

Figs. 5 and 6 indicate that the as-received, reduced, and oxidized 1cPt/SrTiO₃ samples all exhibit catalytic activities to methanol decomposition and partial oxidation (oxy-reforming), resulting in slight changes in conversion and selectivity. The XANES analyses in Figs. 3 and 9 show that Pt in the as-received catalyst is present as either Pt⁴⁺ or Pt²⁺, Pt in the reduced catalyst is completely Pt⁰, and Pt in the oxidized catalyst cooling to 250 °C is nearly all Pt²⁺. Ubago-Perez et al. studied the effect of pretreatment of their activated-carbon-supported Pt catalyst on catalyst characteristics and performance [11]. They pretreated the catalyst in He or H₂ at 400 °C before characterization and reaction. The results indicate that the catalyst pretreated in H₂ resulted in larger Pt particle size, broader particle size distribution, and much less metal dispersion, but higher methanol conversion in the decomposition reaction. In their later paper on partial oxidation, Ubago-Perez et al. reported similar results. They concluded that the larger Pt particles favor improvement of the catalytic activity in both reactions, as well as the selectivity for H₂ and CO [20]. Cao et al. made an O₂-covered catalyst by flowing O₂ over a reduced Pt/Al₂O₃ catalyst and observed the presence of formate when the catalyst was

Table 3
Methanol conversion rate and H₂, CO, and CO₂ production rate in methanol partial oxidation over 1cPt/SrTiO₃.

	Methanol conversion rate (μmol/g/s)	O ₂ conversion (%)	H ₂ production rate (μmol/g/s)	CO production rate (μmol/g/s)	CO ₂ production rate (μmol/g/s)
200 °C	149	97.6	36.5	4.60	37.6
250 °C	313	91.9	199	63.3	80.4
300 °C	549	100	808	345	130
350 °C	698	100	1280	566	161

exposed to methanol [21]. They also observed formate formation on the Al₂O₃ support. The decomposition of formate would give rise to CO₂. We did not see CO₂ formation in methanol decomposition in our oxidized catalyst. Our oxidized and reduced catalysts behaved similarly in methanol decomposition. Compared with the as-received catalyst, they resulted in less methanol conversion and less H₂ and CO selectivity. The oxidized catalyst showed different performance in the methanol partial oxidation (Fig. 6) – less methanol and O₂ conversion and higher H₂ and CO₂ selectivity. It is speculated that, in the decomposition reaction, the formation of CO suppresses the difference between the reduced and oxidized catalysts. However, the presence of O₂ in the partial oxidation reaction maintains this difference. Matolin et al. observed a strong reducing ability of methanol in its adsorption and desorption on Pt/CeO₂ (1 1 1) catalyst [6]. Using X-ray photoelectron spectroscopy and soft X-ray synchrotron radiation photoelectron spectroscopy, they detected the transition of Ce⁴⁺ → Ce³⁺ and an increase of the electron state occupancy for the Ce 4f orbital. This reducing ability of methanol can be used to explain how the 1cPt/SrTiO₃ catalyst as-received from ALD or oxidized before methanol decomposition has catalytic activity.

Unlike what was observed in the earlier experiments on methanol adsorption and decomposition under vacuum [6,7], the present *in situ* XANES of the Pt L3 edge do not fully reveal the reaction mechanism steps of methanol decomposition and partial oxidation over 1cPt/SrTiO₃. Comparing the ΔXANES spectrum obtained in methanol reaction (either decomposition or partial oxidation) and that obtained in CO adsorption over the respective catalyst that had been subjected to various pretreatments or no pretreatment, we found that they indicated the same trend of change in CO coverage. Regardless of the initial Pt state of the catalyst and the adsorption orientation of methanol on the catalyst, methanol finally becomes CO adsorbed on the Pt particle surfaces. Based on periodic DFT calculation, Desai et al. and Niu et al. concluded that the final products of methanol decomposition on Pt particles are adsorbed CO and H [4,5]. Desai et al. also predicted that the adsorbed CO may lead to catalytic poisoning because the adsorption energy is as strong as – 168 kJ/mol [4]. However, we did not notice any trend of catalyst deactivation even in a relatively longer run (about 10 h time on stream). Over the Pt nanoparticle surface, steps of methanol adsorption, C–H and O–H bond disassociation, H₂ formation on the metal surface, and CO and H₂ desorption formed a flux. The trace amount of methane detected may come from methanation [10]. The difference in methanol conversion and product selectivity resulting from as-received 1cPt/SrTiO₃ catalyst on the one hand and reduced and oxidized catalysts on the other may be attributed to the difference in crystalline structures among these samples. This difference needs further study.

5. Conclusion

Our results suggest that SrTiO₃-nanocuboid-supported Pt catalyst, 1cPt/SrTiO₃, consists of highly dispersed Pt nanoparticles with

(1 1 1) crystalline surface and has excellent catalytic activity and hydrogen selectivity for methanol decomposition and partial oxidation. The as-received, reduced, and oxidized catalysts result in noticeable differences in methanol conversion and product selectivity. Temperature has a strong effect on catalytic performance. CO adsorbed on Pt sites is the predominant species on the catalyst surface during both reactions. However, it does not lead to catalytic deactivation. This finding supports the reaction mechanism of dominant C–H and O–H disassociation followed by the formation of CO. Subsequently, CO₂ is formed by CO oxidation when O₂ is present. CH₄ may be formed from methanation.

Acknowledgments

This material is based upon work supported as part of the Institute for Atom-efficient Chemical Transformations (IACT), an Energy Frontier Research Center funded by the U.S. Department of Energy, Office of Science, Office of Basic Energy Sciences. Support for H. Wang was provided by the University of Saskatchewan and Argonne National Laboratory.

References

- [1] D. Hotza, J.C. Diniz da Costa, *Intl. J. Hydrogen Energy* 33 (2008) 4915.
- [2] S. Sá, H. Silva, L. Brandão, J. Sousa, A. Mendez, *Appl. Catal. B: Environ.* 99 (2010) 43.
- [3] T. Schultz, S. Zhou, K. Sundmacher, *Chem. Eng. Technol.* 24 (2001) 1223; S.K. Desai, M. Neurock, K. Kourtakis, *J. Phys. Chem. B* 106 (2001) 2559.
- [4] C.-Y. Niu, J. Jiao, B. Xing, C.-C. Wang, X.-H. Bu, *J. Comput. Chem.* 31 (2010) 2023.
- [5] V. Matolín, V. Johánek, M. Škoda, N. Tsud, K.C. Prince, T. Skála, I. Matolínová, *Langmuir* 26 (2010) 13333.
- [6] I. Matolínová, V. Johánek, J. Mysliveček, K.C. Prince, T. Skála, M. Škoda, N. Tsud, M. Vorokhta, V. Matolín, *Surf. Interface Anal.* 43 (2011) 1325.
- [7] J.C. Brown, E. Gulari, *Catal. Commun.* 5 (2004) 431.
- [8] J.R. Croy, S. Mostafa, H. Heinrich, B.R. Vuenya, *Catal. Lett.* 131 (2009) 21.
- [9] S. Mostafa, J.R. Croy, H. Heinrich, B.R. Vuenya, *Appl. Catal. A: General* 366 (2009) 353.
- [10] R. Ubago-Peréz, F. Carradco-Marín, C. Moreno-Castilla, *Appl. Catal. A: General* 275 (2004) 119.
- [11] F.A. Rabuffetti, H.-S. Kim, J.A. Enterkin, Y. Wang, C.H. Lanier, L.D. Marks, K.R. Roepelmeier, P.C. Stair, *Chem. Mater.* 20 (2008) 5628.
- [12] J. Lu, Y. Lei, J.W. Elam, Atomic layer deposition of noble metals—new developments in nanostructured catalysts, in: Y.-H. Su (Ed.), *Noble Metals, 2012* (Chapter 8).
- [13] J.A. Enterkin, W. Setthapun, J.W. Elam, S.T. Christensen, F.A. Rabuffetti, L.D. Marks, P.C. Stair, K.R. Poepelmeier, C.L. Marshall, *ACS Catal.* 1 (2011) 629.
- [14] S.T. Christensen, H. Feng, J.L. Libera, N. Guo, J.T. Miller, S.T. Christensen, J.W. Elam, *Nano Lett.* 10 (2010) 3047.
- [15] T. Huizinga, J. van Grondelle, R. Prins, *Appl. Catal.* 10 (1984) 199.
- [16] B. Lin, J. Wang, P.H.C. Camargo, M. Jiang, M.J. Kim, Y. Xia, *Nano Lett.* 8 (2008) 2535.
- [17] J.A. Rossin, *J. Mol. Catal.* 58 (1990) 363.
- [18] T. Wu, D.J. Childers, G. Gomez, A.M. Karim, N.M. Schweitzer, A.J. Kropf, H. Wang, T.B. Bolin, Y. Hu, L. Kovarik, R.J. Meyer, J.T. Miller, *ACS Catal.* 2 (2012) 2433.
- [19] R. Ubago-Peréz, F. Carradco-Marín, C. Moreno-Castilla, *Catal. Today* 123 (2007) 158.
- [20] C. Cao, K.L. Hohn, *Catal. A: General* 354 (2009) 26.